

RESEARCH ARTICLE



ISSN: 2321-7758

THE DYNAMIC PERFORMANCE OF DFIG DURING VOLTAGE SAG AND SWELL USING SMES

GOPINATH PULICHERLA¹, L.VEERAKOTLU²

¹PG Student, Department of EEE, NOVA COLLEGE OF Engg & TECHNOLOGY, VIJAYAWADA, India

²Asst Professor, Department of EEE, NOVA COLLEGE OF ENGG & TECHNOLOGY, VIJAYAWADA, India

Article Received: 26/11/2014

Article Revised on: 12/12/2014

Article Accepted on: 20/12/2014



GOPINATH PULICHERLA



L.VEERAKOTLU

ABSTRACT

The integration of wind turbines into modern power grids has significantly increased during the last decade. Wind turbines equipped with doubly fed induction generators (DFIGs) have been dominating wind power installation worldwide since 2002. In this paper, a superconducting magnetic energy storage (SMES) unit is proposed to improve the dynamic performance of a wind energy conversion system equipped with DFIG during voltage sag and voltage swell events. The converter and the chopper of the SMES unit are controlled using a hysteresis current controller and a fuzzy logic controller, respectively. Detailed simulation is carried out using MATLAB/SIMULINK software to highlight the impact of the SMES unit in improving the overall system performance under voltage sag and voltage swell conditions.

Index terms- Doubly fed induction generator (DFIG), fuzzy logic, hysteresis current controller (HCC), superconducting magnetic energy storage (SMES), voltage sag, voltage swell and wind energy conversion system (WECS).

©KY Publications

INTRODUCTION

Utilization of renewable energy sources is becoming more attractive due to the detrimental impact of conventional energy resources on the environment. Implementation of carbon tax in some countries has also been considered as a trigger to accelerate the utilization of renewable energy sources [1]. One of the most promising renewable energy sources is wind energy, which has grown rapidly from about

2000 MW at the end of the year 1990 to 94000 MW by the end of the year 2007. The future prospects of the global wind industry are very encouraging, and it is estimated to grow by more than 70% to reach 160 GW by the year 2012. It is estimated that, by the year 2020, wind power will supply at least 10% of global electricity demands [2]. Owing to the rapid development of power electronics technology, the

number of wind turbines equipped with converter stations has increased. The doubly fed induction generator (DFIG) is one of the most popular variable speed wind turbine generators (WTGs). In this technology, the rotor winding is connected to a coupling transformer through a back-to-back partial-scale voltage source converter (VSC), whereas the stator winding is directly connected to the grid at a point of common coupling (PCC) through the coupling transformer. The VSC decouples the mechanical and electrical frequencies and make variable-speed operation possible [3]. Global trend shows that the market share of the installed wind energy conversion system (WECS) has been dominated by DFIG-based wind turbines since 2002 [4]. In the earlier stages of integrating WECSs into the electricity grids, WTGs were disconnected from the grid during faults at the grid side to avoid any possible damages to wind turbines. There are two strategies that can be applied to improve the performance or the fault ride through (FRT) capability of the DFIG. First is by developing new control techniques to fulfill the criterion of the transmission system operators, as presented in most of the literature [6]–[10]. However, this strategy is effective for new installation and new connection of WECSs to the grid. Second is by applying FACTS

devices or storage energy systems [11], which are a more cost effective choice for existing WECSs. Variable speed WECSs such as DFIG were introduced to overcome the weakness of the fixed speed type in capturing maximum wind energy and to contribute in supplying reactive power to the grid when required [12]. Moreover, during grid fault, voltage drop at the DFIG terminal, high current flow at both grid and rotor side converters, and high voltage across the dc link capacitor may lead to converter station blocking. This condition will be ended by the disconnection of the DFIG from the system. If the DFIG contributes in delivering a large portion of power to the grid, financial loss will be uncountable. Most of the studies about the DFIG are concerned about the improvement of its FRT capability during voltage sag [6]–[10]. No attention however is given to improve the DFIG performance under voltage sag and voltage swell conditions using the same controller. Although the swell event in the grid side is rarely to occur, it can cause voltage rise at the PCC that may violate the grid codes' requirements. Recently, the maximum voltage ride through of Spain [13] and Australia's [14] grid codes is set to 1.3 pu. If the voltage profile at the PCC rises above 1.3 pu, the WTGs have to be disconnected from grid.

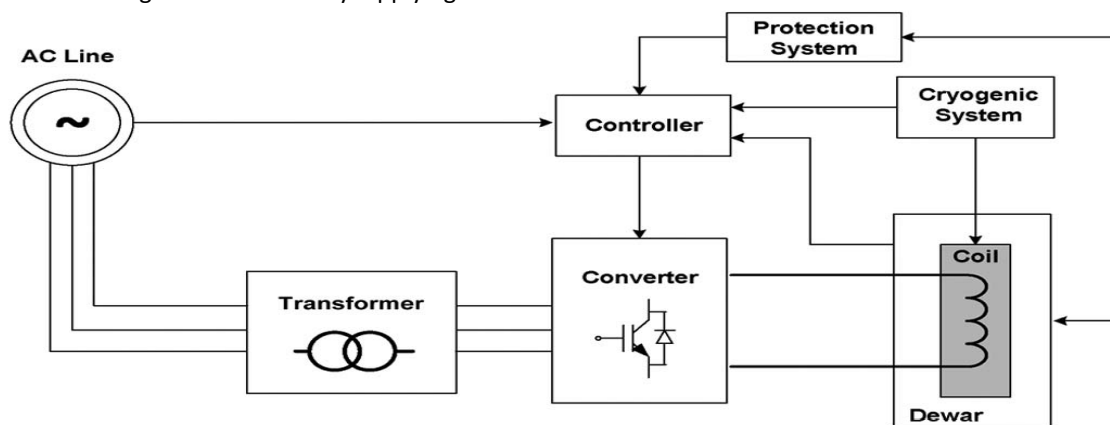


Fig.1 Typical schematic diagram of an SMES unit.

Since the successful installation of the 30-MJ superconducting magnetic energy storage (SMES) unit at Bonneville power administration, Tacoma, in 1982 [15], SMES has attracted many researchers to study its potential applications in power systems [16]–[18]. There are many papers in the literature

that investigated the application of SMES to WECSs. However, most of these studies have only focused on the use of the SMES unit to smooth the output power of fixed-speed WECSs during wind speed fluctuation to avoid system instability [19]–[26]. This paper presents a new application of the SMES unit

to improve the performance of a wind turbine equipped with DFIG during voltage sag and voltage swell at the grid side. A new control system for the SMES unit based on hysteresis current control in conjunction with fuzzy logic control is proposed. The Simulink/ software is used to simulate the wind turbine, the SMES unit, and the model under study. Results are analyzed to highlight the improved dynamic performance of WECSs in conjunction with the SMES unit.

II SMES

An SMES system consists of a superconductor coil, a power-conditioning system, a cryogenic refrigerator, and a cryostat/vacuum vessel to keep the coil at a low temperature required maintaining it in superconducting state. This configuration makes SMES highly efficient in storing electricity with typical efficiency in the range of 95%–98%. Other advantages of the SMES unit include very quick

response and possibilities for high-power applications .A typical SMES configuration is shown in Fig. 1.

III. SYSTEM UNDER STUDY

The system under study shown in Fig. 2(a) consists of six 1.5-MW DFIGs connected to the ac grid at the PCC. The DFIG consists of an induction generator with stator winding connected directly to the grid through a Y/Δ step-up transformer, whereas the rotor winding is connected to a bidirectional back-to-back insulated gate bipolar transistor (IGBT) VSC, as shown in Fig. 2(b). The grid that is represented by an ideal three-phase voltage source of constant frequency is connected to the wind turbines via a 30-km transmission line and Δ/Y step-up transformer. The SMES unit is connected to the 25-kV bus and is assumed to be fully charged at its maximum capacity of 1.0 MJ Tables I and II.

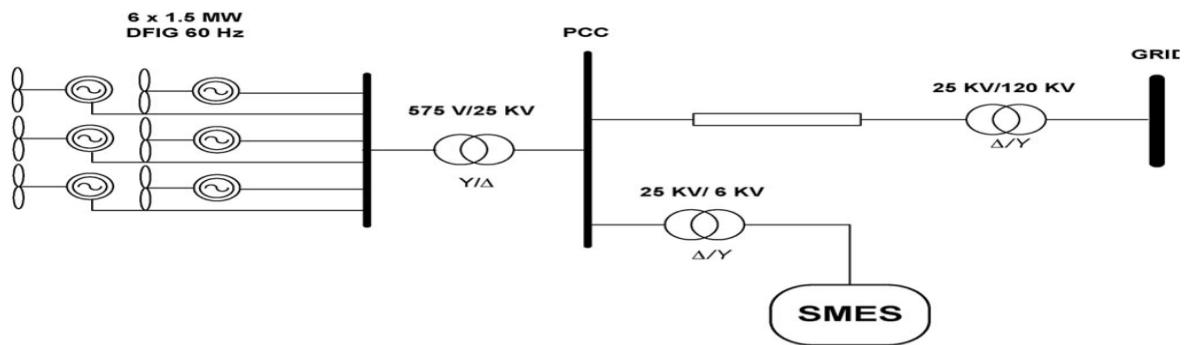


Fig. 2. (a) System under study

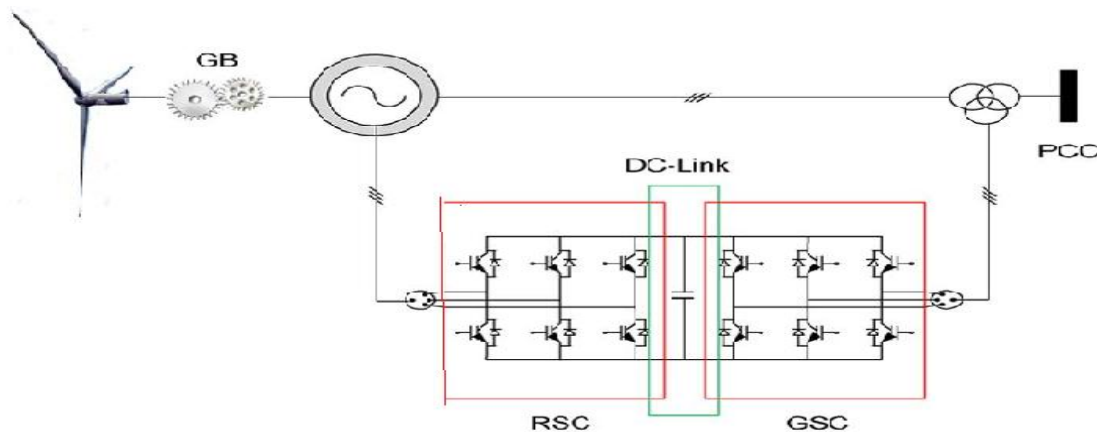


Fig 2(b) Typical configuration of an individual DFIG

TABLE-I: PARAMETERS OF THE DFIG

Duty Cycle (D)	SMES Coil Action
$D = 0.5$	standby condition
$0 \leq D < 0.5$	discharging condition
$0.5 < D \leq 1$	charging condition

TABLE-II: PARAMETERS OF THE TRANSMISSION LINE

RATED POWER	9 MW (66 X @1.5MW)
STATOR VOLTAGE	575V
FREQUENCY	60 HZ
R_S	0.023 PU
R_R	0.016 PU
V_{DC}	1150V

IV. SMES CONTROL APPROACHES

Generally, there are two major configurations of SMES, i.e., current source converter (CSC) and VSC. Traditionally, CSC is connected through a 12-pulse converter configuration to eliminate the ac-side fifth and seventh harmonic currents and the dc side sixth harmonic voltage, thus resulting in significant savings in harmonic filters [18]. The VSC, on the other hand, must be connected with a dc-dc chopper through a dc link, which facilitates energy exchange between the SMES coil and the ac grid. Reference [31] estimates the total cost of the switching devices of the CSC to be 173% of the switching devices and power diodes required for equivalent capacity of the VSC and the chopper. The use of IGBTs in this configuration is more beneficial than GTO since the switching frequency of an IGBT lies on the range of 2–20 kHz, whereas, in case of GTO, the switching frequency cannot exceed 1 kHz [4]. The proposed SMES configuration used in this paper consists of a VSC and dc-dc chopper, as shown in Fig. 3. The converter and the chopper are controlled using a hysteresis current controller (HCC) and a fuzzy logic controller (FLC), respectively. The stored energy in the SMES coil can be calculated as

$$E = \frac{1}{2} I_{SMES}^2 L_{SMES} \quad \text{----- (1)}$$

where E , I_{SMES} , and L_{SMES} are the stored energy, current, and coil inductance of the SMES unit, respectively. While the control system of the dc-dc chopper is presented in [32], the control approach for the VSC as part of the SMES configuration is not presented. In contrast with the dc-dc chopper control system is not presented. be only appropriate for new WECS installations. Application of the SMES system to micro grids is presented in [34], where the SMES is used to stabilize the entire micro grid system. The control scheme presented in this work is very complex because it is working for three different levels of controls; this will lead to high implementation and maintenance cost. Moreover, it requires a robust computational system. The proposed control algorithm in this paper is much simpler and closer to realistic applications, compared with the similar controller proposed .

The control scheme in this paper comprises only two PI controllers and considers the SMES coil current to take the SMES stored energy capacity into account, along with the DFIG generated power as control parameters to determine the direction and level of power exchange between the SMES coil and the ac system. This control system is efficient, simple, and easy to implement, as will be elaborated here.

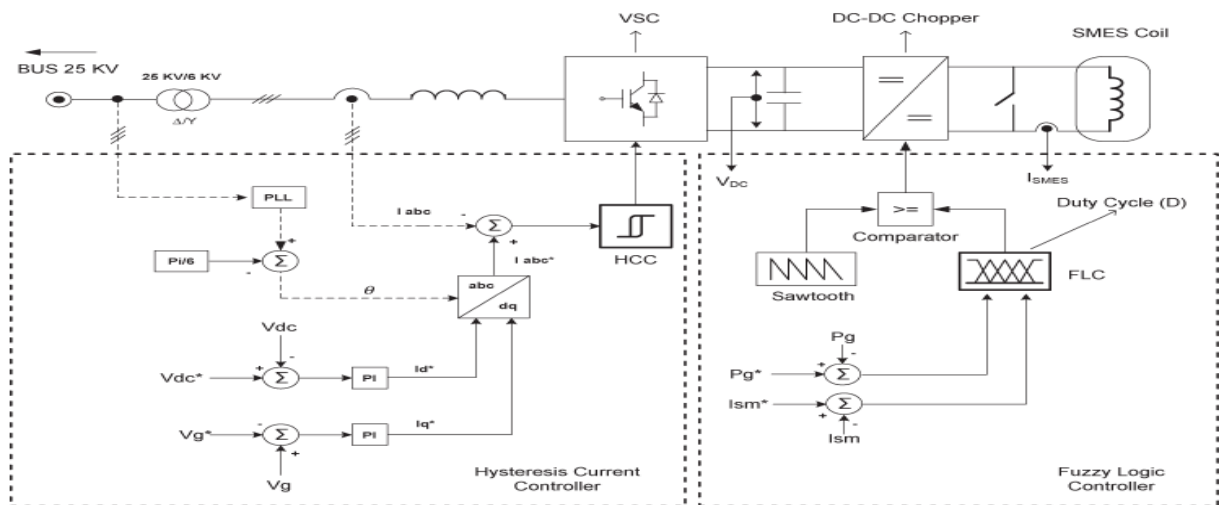


Fig. 3. SMES Configuration and the proposed HCC-FLC control scheme.

A. HCC

The HCC is widely used because of its simplicity, insensitivity to load parameter variations, fast dynamic response, and inherent maximum-current-limiting characteristic. The basic implementation of the HCC is based on deriving the switching signals from the comparison of the actual phase current with a fixed tolerance band around the reference current associated with that phase. The effect of interference between phases referred to as inter phase dependence can lead to high switching frequencies. To maintain the advantages of the hysteresis methods, this phase dependence can be

minimized by using the phase-locked loop (PLL) technique to maintain the converter switching at a fixed predetermined frequency level [37]. The proposed SMES with an auxiliary PLL controller is shown in Fig. 3. The HCC is comparing the three-phase line currents (I_{abc}) with the reference currents (I^*_{abc}), which is dictated by the I^*_d and I^*_q references. The values of I^*_d and I^*_q are generated through conventional PI controllers based on the error values of V_{dc} and V_s . The value of I^*_d and I^*_q is converted through Park transformation ($dq0 - abc$) to produce the reference current (I^*_{abc}).

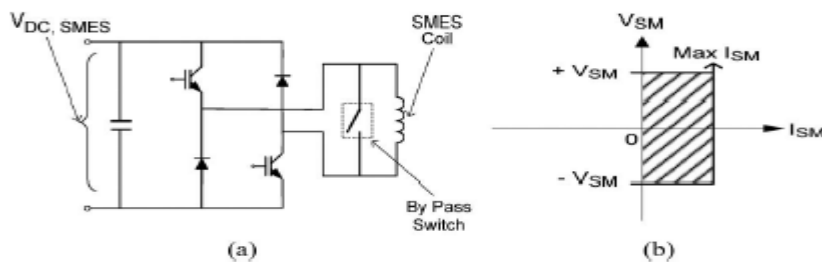


Fig.4. (a) Class-D dc-dc chopper topology with an SMES coil. (b) Operation ranges of the SMES coil

B. FLC

To control power transfer between the SMES coil and the ac system, a dc-dc chopper is used, and fuzzy logic is selected to control its duty cycle (D), as shown in Fig. 3. The FLC is developed according to the fuzzy inference flowchart shown in Fig. 4, which is a process of formulating the mapping from a given input to the designated output. Input variables for the model are the real power generated by the DFIG

and the SMES coil current. The output of the FLC is the duty cycle (D) for a class-D dc-dc chopper that is shown in Fig. 4(a). The $V-I$ operational range for the SMES coil is shown in Fig 4(b). The duty cycle determines the direction and the magnitude of the power exchange between the SMES coil and the ac system, as presented in Table III. If the duty cycle (D) is equal to 0.5, no action will be taken by the coil, and the system is under normal operating

conditions. Under this condition, a bypass switch that is installed

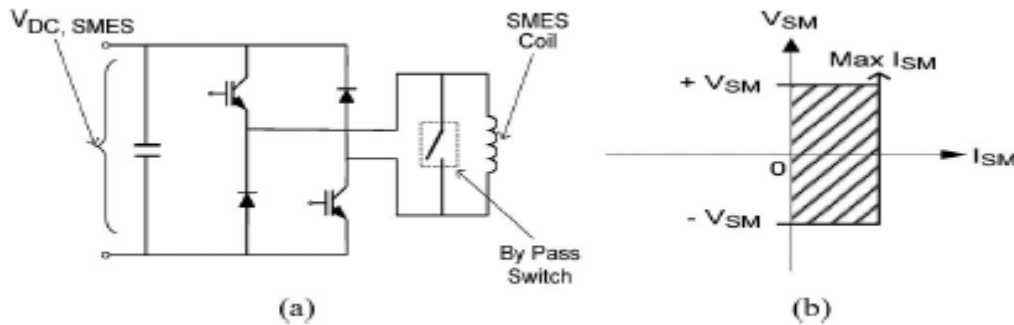


Fig. 5. (a) Class-D dc-dc chopper topology with an SMES coil. (b) Operation range of the SMES coil.

TABLE-III RULES OF THE DUTY CYCLE

$R_1, R_0 (\frac{\Omega}{KM})$	0.1153, 0.413
$L_1, L_0 (H/KM)$	$1.05 \times 10^{-3}, 3.32 \times 10^{-3}$
$C_1, C_0 (F/KM)$	$11.33 \times 10^{-9}, 5.01 \times 10^{-9}$

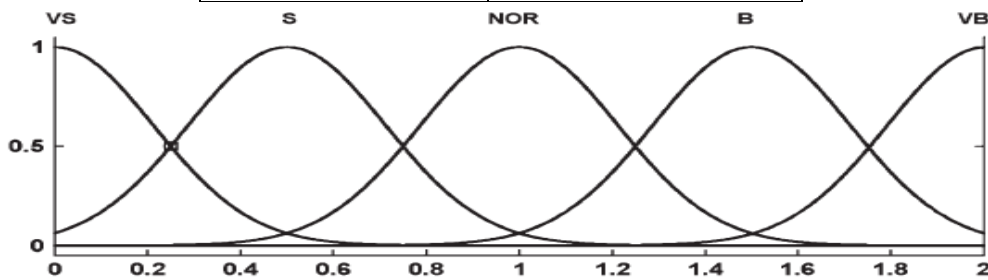


Fig. 6 MF for the input variable PG (pu).

across the SMES coil [shown in Fig. 5(a)] will be closed to avoid the draining process of SMES energy during normal operating conditions. The bypass switch is controlled in such a way that it will be closed if D is equal to 0.5; otherwise, it will be opened. This technique has been introduced in some studies in the literature [21], [31]. When the grid power is reduced, D will be reduced accordingly to be in the range of 0–0.5, and the stored energy in the SMES coil will be transferred to the ac system. The charging process of the SMES coil takes place when D is in the range of 0.5–1.

$$V_{SMES} = (1 - 2D)V_{DC,SMES} \quad \text{-----}(2)$$

where V_{SMES} is the average voltage across the SMES coil, D is duty cycle, and $V_{DC,SMES}$ is the average voltage across the dc-link capacitor of the SMES configuration. The model is built up using the graphical user interface tool provided by MATLAB. Each input was fuzzified into five sets of Gauss-type membership function (MF). The Gaussian curve is a function of a vector x and depends on parameters

$$f(x; \sigma, c) = e^{-\frac{(x-c)^2}{2\sigma^2}} \quad \text{-----}(3)$$

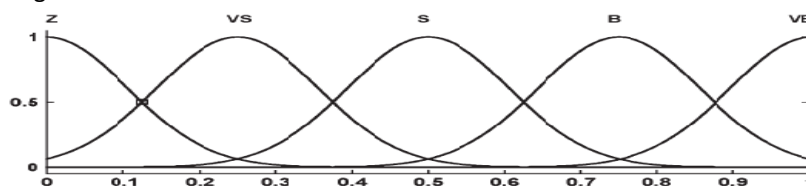


Fig.7. MF for the input variable I_{SMES} (pu)

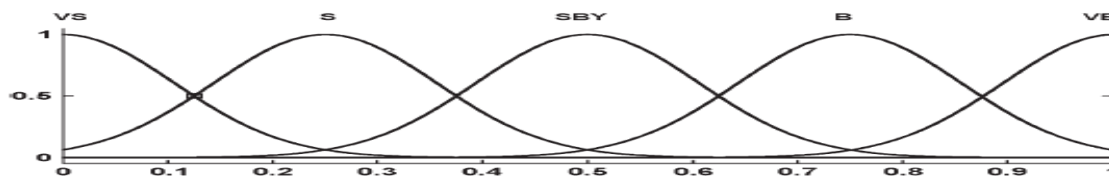


Fig.8.MF for the output variable D(duty cycle).

*V SIMULATION RESULT AND DISCUSSION
 AVOLTAGE SAG EVENT*

A voltage sag depth of 0.5 pu lasting for 0.05 s is applied at $t = 2$ s at the grid side of the system under study. Without the SMES unit, the real power produced by the DFIG will drop to 0.6 pu, and it reaches a maximum overshooting of 40% during the clearance of the fault. SMES unit and during the event of voltage sag, the reactive power support by the DFIG is reduced, and the steady-state condition is reached faster, compared to the system without SMES. The voltage at the PCC is shown in Fig. 10(c), where without SMES, voltage will drop to 0.6 pu. However, by connecting the SMES unit, voltage drop at the PCC will be reduced to only 0.8 pu, which will lead to a voltage drop at the generator terminal to a level of 0.8 pu, which is reference the generator speed will accelerate and oscillate without the SMES unit; however, with the SMES connected to the system, the power drop is reduced, the settling time of the generator speed is substantially reduced, and the overshooting level is significantly decreased. Another effect of the voltage sag on the DFIG's behavior is on the voltage across the DFIG dc link capacitor that is shown in Fig. 10(e). The voltage overshoot across the dc-link capacitor during fault clearance is slightly reduced with the SMES unit connected to the system.

Voltage SWELL Event

Voltage swell can occur due to switching off a large load or switching on a large capacitor bank. In this simulation, a voltage swell is applied by increasing the voltage level at the grid side to 1.5 pu. The voltage swell is assumed to start at $t = 2$ s and lasts for 0.05 s. In this event, the DFIG-generated power will increase upon the swell occurrence and will be reduced when it is cleared.

Without the connection of the SMES unit, the voltage across the DFIG dc-link capacitor will experience significant oscillations and overshooting

level upon voltage swell incidence, as can be shown in Fig. 11(e). In some occasions, this may lead to the blocking of the converters. As shown in Fig. 11(e), voltage oscillations, as well as voltage overshooting level, are significantly reduced by connecting the SMES unit to the system.

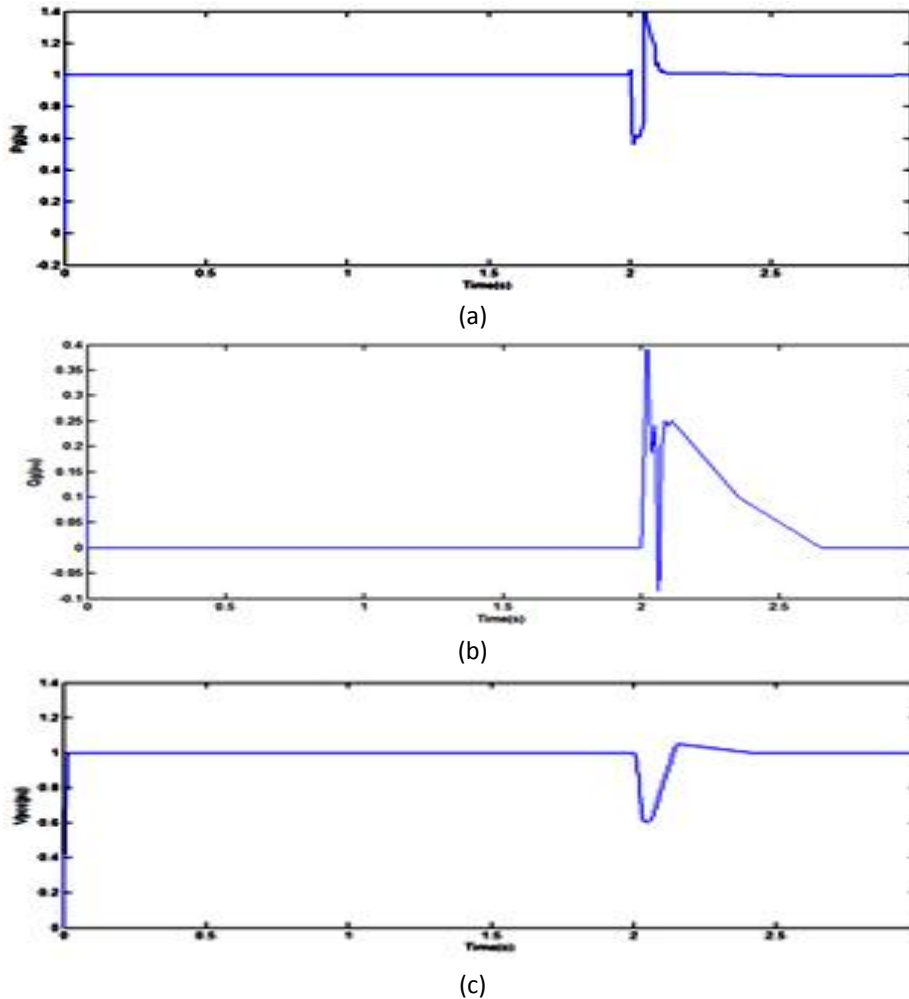
C. SMES Responses during Voltage Sag and Swell

In both voltage sag and voltage swell events, voltage across the SMES coil will be maintained at zero level once the maximum current in the SMES coil is reached. Once a system with SMES unit has regained post fault stability, the SMES coil is not preferred to be kept on continuously to avoid the draining process of SMES energy during normal operating conditions. Furthermore, turning it off can reduce the generator shaft speed oscillations to some extent. It also reduces the operating expenses of the SMES unit. This is achieved by short circuiting the SMES coil through a bypass switch shown in Fig. 5(a). In both the voltage sag and voltage swell events, it is observed that the voltage across the dc-link capacitor of the SMES configuration ($V_{DC,SMES}$) oscillates in an opposite manner to V_{SMES} , and its level at any time is related to the level of V_{SMES} . The level of V_{SMES} at any time is correlated to the level of $V_{DC,SMES}$ and the duty cycle value by the relation given in (2).

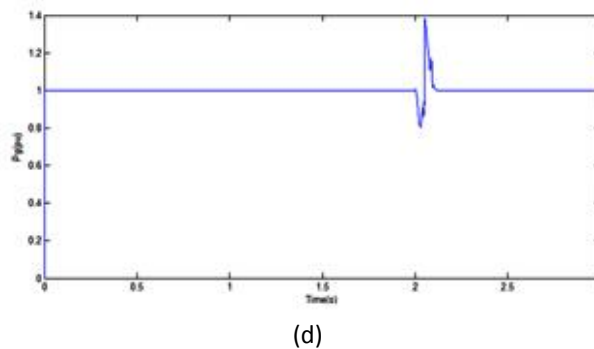
D. SMES Capacity

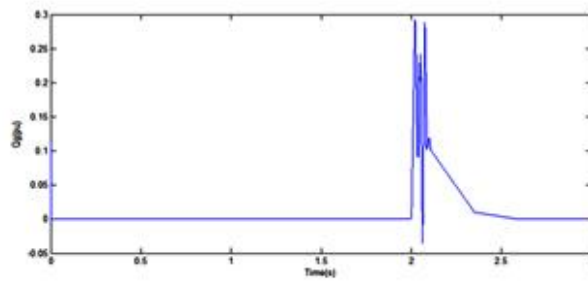
The SMES unit capacity depends on the application and charging/discharging duration. Very high energy rating has excellent impact on damping oscillations rapidly, but the cost of the unit will be too high due to large current in the coil. Meanwhile, if the energy rating is too low, the output of the SMES unit will be limited during disturbances, and it will not be very effective in controlling system oscillations quickly. To make the SMES coil effective in voltage swell events, the rated inductor current is set at a level higher than the nominal coil current [41]. In the system under study, the rated coil current was chosen to be

2.03 kA. This will allow the SMES coil to absorb maximum energy up to 1.03 MJ during the voltage sag event.

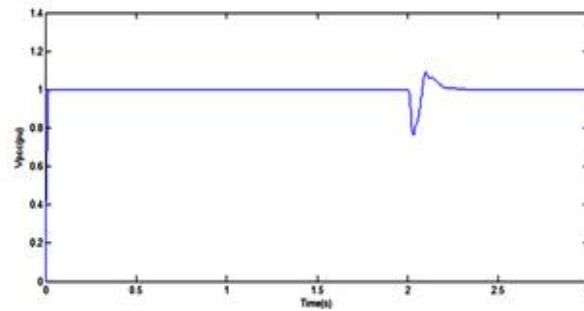


.Fig 9. DFIG response during voltage sag with an SMES unit.(a)active power,(b)reactive power,(c)PCC voltage.



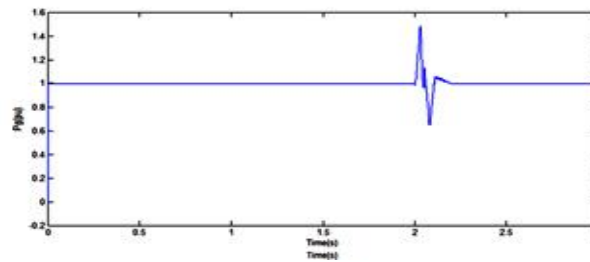


(e)

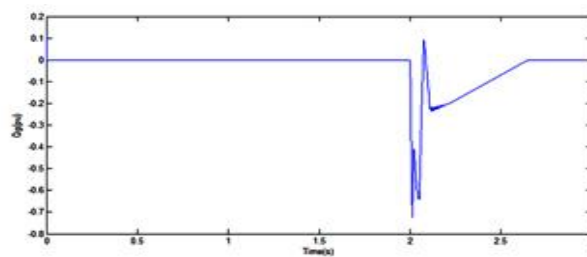


(f)

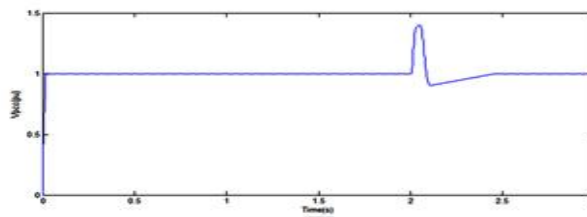
Fig.10.DFIG response during voltage sag without an SMES unit
(d)active power,(e)reactive power,(f)PCC voltage



(a)

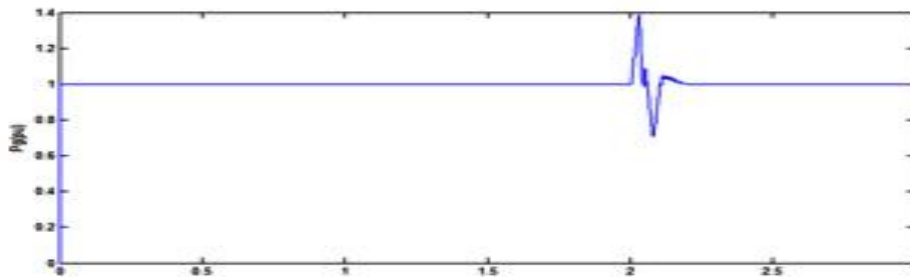


(b)

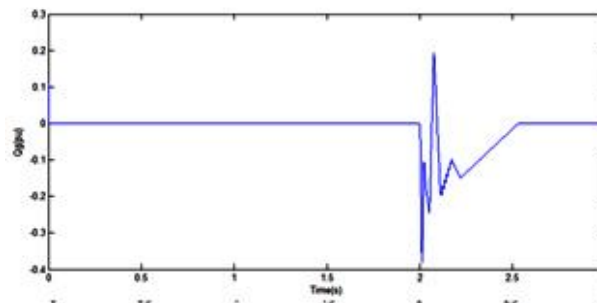


(c)

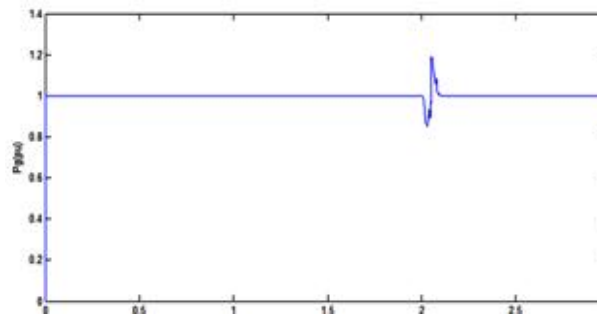
Fig.11.DFIG response during voltage swell without an SMES unit (a)active power,(b)reactive power,(c)PCC voltage



(d)



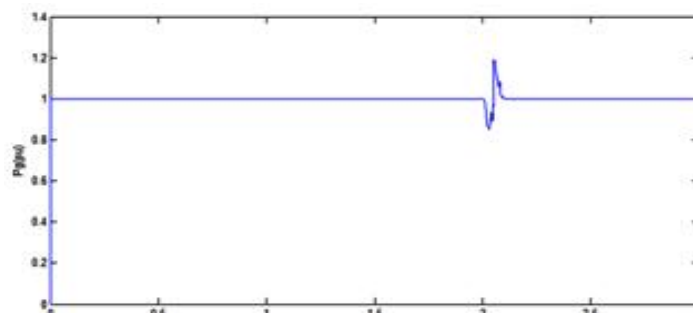
(e)



(f)

Fig.12.DFIG response during voltage swell with an SMES unit. (d)active power,(e)reactive power, (f)PCC voltage.

The extension of this project for voltage sag can be done with is the help of artificial neural network(ANN) which will show the better performance compared with fuzzy logic controller(FLC).The simulation waveforms of active power, reactive power ,PCC voltage as shown below.



(a)

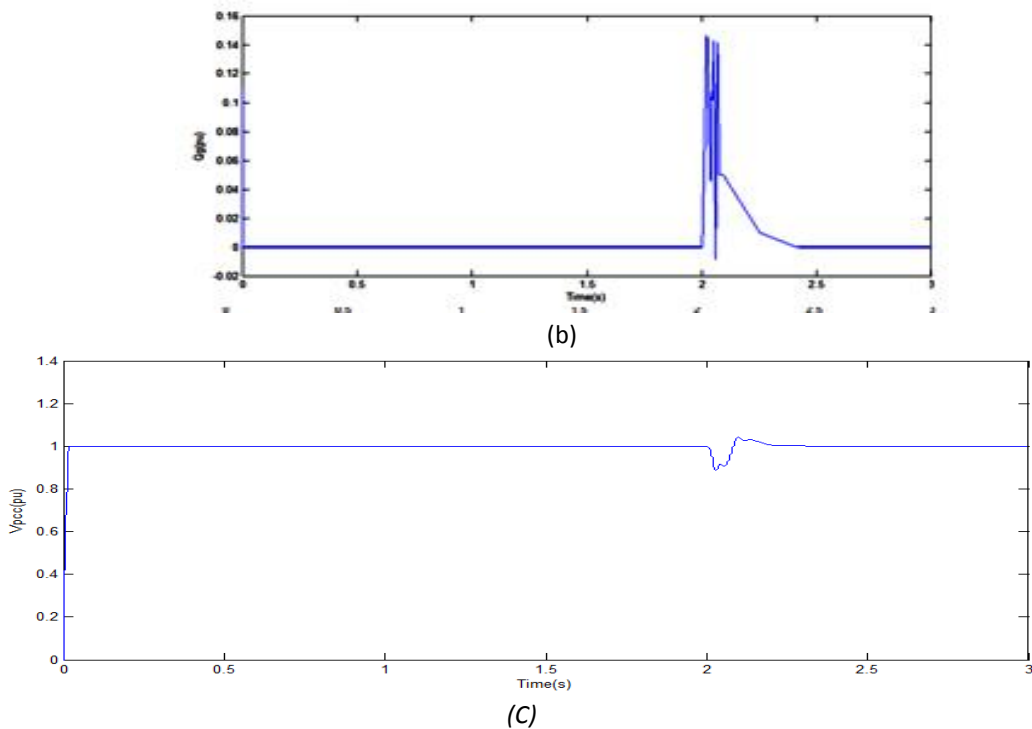


Fig13(a) active power (b) reactive power (c) pcc voltage

CONCLUSION

A new control algorithm along with a new application of the SMES unit to improve the transient response of WTGs equipped with DFIG during voltage sag and voltage swell events has been proposed. Simulation results have shown that the SMES unit is very effective in improving the dynamic performance of a power system with wind turbine equipped with DFIG during voltage sag and voltage swell at the grid side. The proposed control algorithm of the SMES unit is simple and easy to implement and is able to improve the FRT of the DFIG. The SMES unit, on the other hand is still a costly piece of equipment

REFERENCES

[1]. L. Freris and D. Infield, *Renewable Energy in Power Systems*. Wiltshire, U.K.: Wiley, 2008, p. 217.
 [2]. P. Musgrove, *Wind Power*. New York: Cambridge Univ. Press, 2010, pp. 221–222.
 [3]. J. M. Carrasco, L. G. Franquelo, J. T. Bialasiewicz, E. Galvan, R. C. P. Guisado, M. A. M. Prats, J. I. Leon, and N. Moreno-Alfonso, “Power-electronic systems for the grid integration of renewable energy sources: A survey,” *IEEE Trans. Ind.*

Electron., vol. 53, no. 4, pp. 1002–1016, Jun. 2006.
 [4]. T. Ackerman, *Wind Power in Power System*. West Sussex, U.K.: Wiley, 2005, p. 65.
 [5]. M. Tsili and S. Papathanassiou, “A review of grid code technical requirements for wind farms,” *IET Renew. Power Gener.*, vol. 3, no. 3, pp. 308–332, Sep. 2009.
 [6]. S. Seman, J. Niiranen, and A. Arkkio, “Ride-through analysis of doubly fed induction wind-power generator under unsymmetrical network disturbance,” *IEEE Trans. Power Syst.*, vol. 21, no. 4, pp. 1782–1789, Nov. 2006.
 [7]. J. Lopez, E. Gubia, E. Olea, J. Ruiz, and L. Marroyo, “Ride through of wind turbines with doubly fed induction generator under symmetrical voltage dips,” *IEEE Trans. Ind. Electron.*, vol. 56, no. 10, pp. 4246–4254, Oct. 2009.
 [8]. M. Mohseni, S. M. Islam, and M. A. S. Masoum, “Impacts of symmetrical and asymmetrical voltage sags on DFIG-based wind turbines considering phase-angle jump, voltage recovery, and sag

- parameters," *IEEE Trans. Power Electron.*, vol. 26, no. 5, pp. 1587–1598, May 2011.
- [9]. Y. Xiangwu, G. Venkataramanan, P. S. Flannery, W. Yang, D. Qing, and Z. Bo, "Voltage-sag tolerance of DFIG wind turbine with a series grid side passive-impedance network," *IEEE Trans. Energy Convers.*, vol. 25, no. 4, pp. 1048–1056, Dec. 2010.
- [10]. S. Hu, X. Lin, Y. Kang, and X. Zou, "An improved low-voltage ride through control strategy of doubly fed induction generator during grid faults," *IEEE Trans. Power Electron.*, vol. 26, no. 12, pp. 3653–3665, Dec. 2011.
- [11]. J. G. Sloopweg, S. W. H. de Haan, H. Polinder, and W. L. Kling, "General model for representing variable speed wind turbines in power system dynamics simulations," *IEEE Trans. Power Syst.*, vol. 18, no. 1, pp. 144–151, Feb. 2003.
- [12]. F. Blaabjerg and Z. Chen, *Power Electronics for Modern Wind Turbines*. Aalborg, Denmark: Morgan & Claypool, 2006, p. 18.
- [13]. M. Altin, O. Goksu, R. Teodorescu, P. Rodriguez, B. B. Jensen, and L. Helle, "Overview of recent grid codes for wind power integration," in *Proc. 12th Int. Conf. OPTIM*, 2010, pp. 1152–1160.[14] AEMO. [Online].
- [14]. H. J. Boenig and J. F. Hauer, "Commissioning tests of the bonneville power administration 30 MJ superconducting magnetic energy storage unit," *IEEE Trans. Power App. Syst.*, vol. PAS-104, no. 2, pp. 302–312, Feb. 1985.
- [15]. M. H. Ali, W. Bin, and R. A. Dougal, "An overview of SMES applications in power and energy systems," *IEEE Trans. Sustainable Energy*, vol. 1, no. 1, pp. 38–47, Apr. 2010.
- [16]. A. Abu-Siada, "Application of superconducting magnetic energy storage units to improve power system performance," Ph.D. thesis, Dept. Elect. Eng., Curtin Univ. Technol., Bentley, Australia, 2004.
- [17]. A. Abu-Siada and S. Islam, "Application of SMES unit in improving the performance of an AC/DC power system," *IEEE Trans. Sustainable Energy*, vol. 2, no. 2, pp. 109–121, Apr. 2011.
- [18]. J. Hee-Yeol, A. R. Kim, K. Jae-Ho, P. Minwon, Y. In-Keun, K. Seok-Ho, S. Kideok, K. Hae-Jong, S. Ki-Chul, T. Asao, and J. Tamura, "A study on the operating characteristics of SMES for the dispersed power generation system," *IEEE Trans. Appl. Supercond.*, vol. 19, no. 3, pp. 2028–2031, Jun. 2009.
- [19]. S. S. Chen, L. Wang, W. J. Lee, and Z. Chen, "Power flow control and damping enhancement of a large wind farm using a superconducting magnetic energy storage unit," *IET Renew. Power Gener.*, vol. 3, no. 1, pp. 23–38, Mar. 2009.